Forward propagation of time evolving acoustic pressure: Formulation and investigation of the impulse response in time-wavenumber domain

Vincent Grulier, Sébastien Paillasseur, Jean-Hugh Thomas,[a] and Jean-Claude Pascal
Laboratoire d'Acoustique de l'Université du Maine (LAUM UMR-CNRS 6613) and Ecole Nationale Supérieure d'Ingénieurs du Mans, rue Aristote, 72085 Le Mans Cedex 09, France

Jean-Christophe Le Roux
Centre de Transfert de Technologie du Mans, 20 rue Thales de Milet, 72000 Le Mans, France

(Received 11 March 2009; revised 9 August 2009; accepted 10 August 2009)

The aim of this work is to continuously provide the acoustic pressure field radiated from nonstationary sources. From the acquisition in the nearfield of the sources of a planar acoustic field which fluctuates in time, the method gives instantaneous sound field with respect to time by convolving wavenumber spectra with impulse response and then inverse Fourier transforming into space for each time step. The quality of reconstruction depends on the impulse response which is composed of investigated parameters as transition frequency and propagation distance. Sampling frequency also affects errors of the practically discrete impulse response used for calculation. To avoid aliasing, the impulse response is low-pass filtered with Chebyshev or Kaiser–Bessel filter. Another approach to implement the impulse response consists of applying an inverse Fourier transform to the theoretical transfer function for propagation. To estimate the performance of each processing method, a simulation test involving several source monopoles driven by nonstationary signals is executed. Some indicators are proposed to assess the accuracy of the temporal signals predicted in a forward plane. The results show that the use of a Kaiser–Bessel filter numerically implemented or that of the inverse Fourier transform can provide the most accurate instantaneous acoustic signals. © *2009 Acoustical Society of America.* [DOI: 10.1121/1.3216916]

PACS number(s): 43.60.Gk, 43.20.Px, 43.60.Sx [EJS] Pages: 2367–2378

I. INTRODUCTION

Knowledge of the instantaneous acoustic field radiated far from sources is of particular interest in several applications. Among them, active control of the noise radiated by structural bodies requires a monitoring signal in the nearfield or in the farfield to provide appropriate signals to the actuators in order to suppress the noise. In many cases, this control only concerns some components of the radiated field, associated with a spatial representation or with components which can be filtered within the wavenumber spectrum obtained from Fourier transform of the spatial pressure distribution. A representative temporal signal is then necessary for the control algorithm.[1,2] Other applications need a description of the instantaneous radiation (for instance, due to unsteady excitation such as impacts or turbulent flows), whose spatial and time features are of great importance for the acoustic perception of a listener. The applications mainly concern the study of musical instruments, how to model them for sound synthesis,[3,4] although more industrial applications are interested in sound quality. In this field, reducing impact noise is particularly difficult and requires a technique to efficiently characterize the phenomena.[5,6]

We are interested in acquiring or simulating a time-dependent acoustic field using a microphone array in the nearfield of the sources so as to find the time-dependent pressure field in a plane further from the sources. Furthermore, solving this problem would be the first step of a more complex task which consists of reconstructing a nonstationary pressure field directly on a source plane from measurements done in the nearfield as in nearfield acoustic holography involving stationary acoustic sources.[7] The resolution of this inverse problem[8] is not considered in this paper, as the focus is on the direct problem which is forward prediction of acoustic pressure field. In the article, this direct problem is called forward radiation problem.

For harmonic signals (using the Helmholtz integral), a widely used method for calculating the acoustic radiation consists of formulating and solving the problem in the wavenumber domain[7,9] and then transforming back to the spatial domain. To ensure the transition to the spatial domain, some numerical solutions using fast Fourier transforms (FFTs) have been proposed.[10] Among the other possible solutions, working in the wavenumber domain is without doubt the most efficient using the FFT algorithm.[11] With this method, the spatial Fourier transform with respect to both variables x and y of the Helmholtz equation leads to the solution of the equation in the z direction and the prediction of how the wavenumber spectrum propagates in this direction for each angular frequency ω. However, the solution which consists of solving the problem for each spectral component and then synthesizing the temporal signal through an inverse Fourier transform[11] is time consuming and sensitive to errors for the

[a]Author to whom correspondence should be addressed. Electronic mail: jean-hugh.thomas@univ-lemans.fr

low frequency components. Indeed the method requires one Fourier transform with respect to time for each measurement point of the array, one spatial Fourier transform and processing of the wavenumber spectrum for each spectral line, and at last one inverse Fourier transform with respect to time for each measurement point. A fundamentally different approach is presented here which involves the time-wavenumber domain without operating in the frequency domain. After applying a Fourier transform with respect to the planes x and y, an equation along the z axis describes how the instantaneous wavenumber spectrum propagates. This equation is then solved by using the Laplace transform. A similar approach but different in the way of seeking the solution was proposed by Forbes *et al.*[12] providing the same result. The solution can be presented as a convolution product between each component of the wavenumber spectrum and an impulse response obtained analytically in the time-wavenumber domain. This has the advantage of continuously processing the signal so that each new sample picked up by the microphones provides a new sample of the propagated pressure field. This method is the central part of the study presented here where the relevance of the impulse response is tested from nonstationary simulated acoustic sources. The main question to answer is how to implement the impulse response and with what sample rate. We also emphasize the fact that the impulse response should be processed before projecting the input pressure field. Some criteria are finally given to assess the viability of the method and to compare different processing methods applied to the impulse response in the time-wavenumber domain.

The theoretical formulation of the method providing an impulse response in the time-wavenumber domain is given in Sec. II. In spite of the fact that the starting equation is also the wave equation, the presentation of the approach based here on the Laplace formalism differs from that of Forbes *et al.*[12] but leads to the same expression. Then the shape and the frequency response of the impulse response are presented in Sec. III. In particular, an important feature of the impulse response is highlighted. It is the transition frequency which separates for each point of the wavenumber domain two kinds of travelling waves, propagating or decaying. Next, the aim is to implement the impulse response using a finite number of samples. The influence of several parameters such as the propagation distance, the transition frequency, and the sampling frequency is investigated in Sec. IV. Then several processing methods to implement an effective impulse response are described. Most of them are based on low-pass filtering of the response. An approach using the inverse Fourier transform is also mentioned. Numerical results are discussed in Sec. V while the source plane is composed of three monopoles generating nonstationary acoustic signals. Some indicators[13,14] are given to objectively compare the signals forward propagated to another plane.

II. WAVE EQUATION SOLUTION IN TIME-WAVENUMBER DOMAIN

First, the wave equation in Cartesian geometry is considered:

$$\nabla^2 p(x,y,z,t) - \frac{1}{c^2}\frac{\partial^2 p(x,y,z,t)}{\partial t^2} = 0. \tag{1}$$

By applying the Fourier transform with respect to x and y to Eq. (1), using the time-wavenumber spectrum $P(k_x,k_y,z,t)$ given by

$$P(k_x,k_y,z,t) = \int_{-\infty}^{\infty}\int_{-\infty}^{\infty} p(x,y,z,t)e^{j(k_x x+k_y y)}dxdy, \tag{2}$$

Eq. (1) yields

$$\frac{\partial^2 P(k_x,k_y,z,t)}{\partial z^2} - \frac{1}{c^2}\frac{\partial^2 P(k_x,k_y,z,t)}{\partial t^2} - (k_x^2+k_y^2)P(k_x,k_y,z,t) = 0. \tag{3}$$

By setting

$$F(z,t) = P(k_x,k_y,z,t), \quad a = \frac{1}{c^2}, \quad b = k_x^2 + k_y^2, \tag{4}$$

Eq. (3) can be rewritten as

$$\frac{\partial^2 F(z,t)}{\partial z^2} - a\frac{\partial^2 F(z,t)}{\partial t^2} - bF(z,t) = 0. \tag{5}$$

To seek the solution of Eq. (3) for each point (k_x,k_y) of the instantaneous wavenumber spectrum, the Laplace formalism[15] is used with $\mathcal{L}(F(z,t))=f(z,s)$ the Laplace transform of $F(z,t)$. Considering

$$\mathcal{L}\left(\frac{\partial^2 F(z,t)}{\partial z^2}\right) = \frac{\partial^2 f(z,s)}{\partial z^2},$$

$$\mathcal{L}\left(\frac{\partial F(z,t)}{\partial t}\right) = sf(z,s) - F(z,0),$$

$$\mathcal{L}\left(\frac{\partial^2 F(z,t)}{\partial t^2}\right) = s^2 f(z,s) - sF(z,0) - \frac{\partial F(z,0)}{\partial t}, \tag{6}$$

and that the initial condition $(t=0)$ is zero, as the solution sought is an impulse response,

$$F(z,0) = 0, \tag{7}$$

the Laplace transform of Eq. (5) yields

$$\frac{\partial^2 f(z,s)}{\partial z^2} - (as^2+b)f(z,s) = 0. \tag{8}$$

The general solution of Eq. (8) is

$$f(z,s) = Ke^{\alpha z}, \tag{9}$$

where K and α are two constants which need to be found.

Substituting Eq. (9) into Eq. (8) leads to two possible values for α:

$$\alpha = \pm\sqrt{as^2+b}. \tag{10}$$

Since waves propagate toward the increasing z axis and since it is assumed that there is no reflective wave, the solution chosen for α is the negative one,

$$\alpha = -\sqrt{as^2+b}. \tag{11}$$

K is given by the initial condition for $z=0$,

$$K = f(0,s). \tag{12}$$

Hence after substituting Eqs. (11) and (12) into Eq. (9), the solution for $f(z,s)$ becomes

$$f(z,s) = f(0,s)e^{-z\sqrt{as^2+b}}. \tag{13}$$

According to Hladik,[15] the exponential term $e^{-z\sqrt{as^2+b}}$ in Eq. (13) can be expressed as

$$e^{-z\sqrt{as^2+b}} = u(z,s) + v(z,s), \tag{14}$$

where

$$u(z,s) = e^{z\sqrt{as^2}} \tag{15}$$

and

$$v(z,s) = -z\sqrt{b}\int_{z\sqrt{a}}^{\infty} e^{-st}\frac{J_1(\sqrt{b/a}\sqrt{t^2-az^2})}{\sqrt{t^2-az^2}}dt, \tag{16}$$

where J_1 denotes the Bessel function of the first kind and order 1.

Hence Eq. (13) yields

$$f(z,s) = f(0,s)u(z,s) + f(0,s)v(z,s). \tag{17}$$

Considering

$$\mathcal{L}(F(0,t)) = f(0,s),$$

$$\mathcal{L}(V(z,t)) = v(z,s),$$

$$\mathcal{L}(F(z,t-t_0)) = f(z,s)e^{-st_0}, \tag{18}$$

and applying the inverse Laplace transform to Eq. (17), it follows that

$$F(z,t) = \begin{cases} 0 & \text{for } 0 \le t < z\sqrt{a} \\ F(0,t-z\sqrt{a}) + F(0,t) * V(z,t) & \text{for } t \ge z\sqrt{a}, \end{cases} \tag{19}$$

with

$$V(z,t) = \begin{cases} 0 & \text{for } 0 \le t < z\sqrt{a} \\ -z\sqrt{b}\dfrac{J_1(\sqrt{b/a}\sqrt{t^2-az^2})}{\sqrt{t^2-az^2}} & \text{for } t \ge z\sqrt{a}. \end{cases} \tag{20}$$

Since we used the notation given by Eq. (4), hence with $\sqrt{a}=1/c$ and $\sqrt{b}=\sqrt{k_x^2+k_y^2}$, the solution of Eq. (3) for the time-wavenumber spectrum is provided from Eqs. (19) and (20):

$$P(k_x,k_y,z,t) = 0 \quad \text{for } 0 \le t < \frac{z}{c}$$

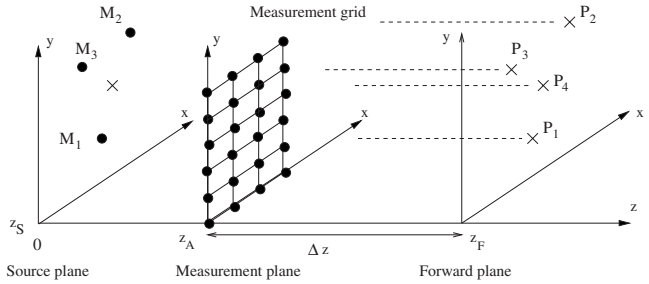

FIG. 1. Geometry of the radiation problem: the pressure field in $z=z_F$ has to be computed from the pressure field acquired in $z=z_A$. The numerical study involves three nonstationary monopoles M_1, M_2, and M_3.

$$P(k_x,k_y,z,t) = P\left(k_x,k_y,0,t-\frac{z}{c}\right) - P(k_x,k_y,0,t) * \left[z\sqrt{k_x^2+k_y^2}\frac{J_1\left(c\sqrt{k_x^2+k_y^2}\sqrt{t^2-\frac{z^2}{c^2}}\right)}{\sqrt{t^2-\frac{z^2}{c^2}}}\Gamma\left(t-\frac{z}{c}\right)\right]$$

$$\text{for } t \ge \frac{z}{c}. \tag{21}$$

Γ is the Heaviside function defined by

$$\Gamma(t) = \begin{cases} 0 & \text{for } t < 0 \\ \frac{1}{2} & \text{for } t = 0 \\ 1 & \text{for } t > 0. \end{cases} \tag{22}$$

For $t \ge z/c$, Eq. (21) can be expressed as a convolution product between the time-wavenumber spectrum $P(k_x,k_y,0,t)$ and an impulse response $h(k_x,k_y,z,t)$:

$$P(k_x,k_y,z,t) = P(k_x,k_y,0,t) * h(k_x,k_y,z,t), \tag{23}$$

where $h(k_x,k_y,z,t)$ is given by

$$h(k_x,k_y,z,t) = \delta\left(t-\frac{z}{c}\right) - z\sqrt{k_x^2+k_y^2}\frac{J_1\left(c\sqrt{k_x^2+k_y^2}\sqrt{t^2-\frac{z^2}{c^2}}\right)}{\sqrt{t^2-\frac{z^2}{c^2}}}\Gamma\left(t-\frac{z}{c}\right). \tag{24}$$

$\delta(t)$ denotes the Dirac distribution.

III. FORWARD PROPAGATION OF TIME EVOLVING PRESSURE FIELD

A. Propagation in the time-wavenumber domain

By considering the geometry of the problem (see Fig. 1), the time-dependent wavenumber spectrum $P(k_x,k_y,z_F,t)$ in a forward plane $z=z_F$ can be obtained by convolving each component of the time-dependent wavenumber spectrum $P(k_x,k_y,z_A,t)$ acquired in a measurement plane $z=z_A$ with an impulse response $h(k_x,k_y,z_F-z_A,t)$ in the time-wavenumber domain:

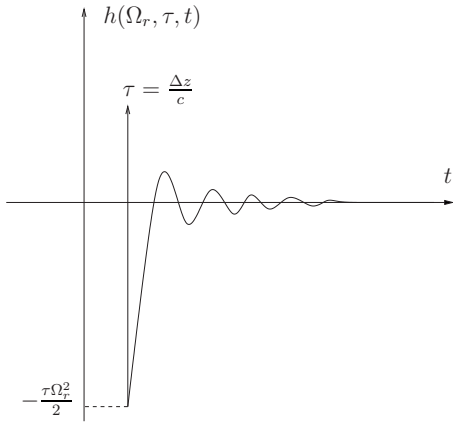

FIG. 2. Shape of the impulse response $h(\Omega_r,\tau,t)$ defined in Eq. (26).

$$P(k_x,k_y,z_F,t)=P(k_x,k_y,z_A,t)*h(k_x,k_y,z_F-z_A,t). \quad (25)$$

By using the following notation for the propagation distance $\Delta z=z_F-z_A$, the wavenumber $k_r=\sqrt{k_x^2+k_y^2}$, the propagation delay $\tau=\Delta z/c$, and the transition pulsation $\Omega_r=ck_r$, the impulse response $h(k_x,k_y,\Delta z,t)$ of Eq. (24) can be rewritten as

$$h(\Omega_r,\tau,t)=\delta(t-\tau)-\tau\Omega_r^2\frac{J_1(\Omega_r\sqrt{t^2-\tau^2})}{\Omega_r\sqrt{t^2-\tau^2}}\Gamma(t-\tau). \quad (26)$$

The theoretical impulse response $h(\Omega_r,\tau,t)$ is represented in Fig. 2. In practical applications, the instantaneous wavenumber spectrum is obtained by processing a two-dimensional spatial Fourier transform at each discrete time of the signals acquired by a microphone array. The pressure field $p(x,y,z,t)$ on the plane $z=z_F$ is obtained by processing an inverse two-dimensional spatial Fourier transform of the result of Eq. (25). The discrete problem is studied in Sec. IV.

B. Interpretation in the frequency domain

The frequency response $H(\Omega_r,\tau,f)$ is the Fourier transform with respect to time of the impulse response $h(\Omega_r,\tau,t)$. It can also be highlighted by applying a Fourier transform to Eq. (25). The obtained equation is then

$$P(k_x,k_y,z_F,\omega)=P(k_x,k_y,z_A,\omega)H(\Omega_r,\tau,\omega). \quad (27)$$

This describes the relationship between the known pressure field on a plane $z=z_A$ and the pressure on any other plane $z=z_F$ when the studied stationary acoustic sources are confined on the half plane $z\leq z_S$ ($z=z_S$ is the source plane),[7]

$$P(k_x,k_y,z_F,\omega)=P(k_x,k_y,z_A,\omega)G_P(k_r,\Delta z,\omega), \quad (28)$$

where the propagator G_P is defined by

$$G_P(k_r,\Delta z,\omega)=e^{-jk_z\Delta z}=\begin{cases}e^{-j\Delta z\sqrt{(\omega/c)^2-k_r^2}} & \text{for } \dfrac{\omega}{c}\geq k_r\\ e^{-\Delta z\sqrt{k_r^2-(\omega/c)^2}} & \text{for } \dfrac{\omega}{c}<k_r,\end{cases} \quad (29)$$

where c is the sound speed.

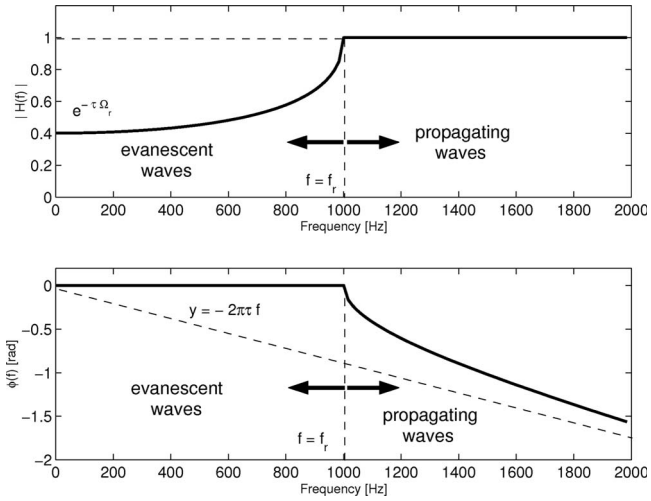

FIG. 3. Magnitude and phase in rad of the theoretical transfer function $H(\Omega_r,\tau,f)$ for the transition frequency $f_r=1000$ Hz and the propagation distance $\Delta z=0.05$ m.

By using Eqs. (27)–(29), the frequency response $H(\Omega_r,\tau,\omega)$ can be written as

$$H(\Omega_r,\tau,\omega)=G_P(\Omega_r,\tau,\omega)=\begin{cases}e^{-j\tau\sqrt{\omega^2-\Omega_r^2}} & \text{for } \omega\geq\Omega_r\\ e^{-\tau\sqrt{\Omega_r^2-\omega^2}} & \text{for } \omega<\Omega_r.\end{cases} \quad (30)$$

The magnitude and the phase of the frequency response are represented in Fig. 3 for a transition frequency $f_r=\Omega_r/2\pi=1000$ Hz and $\Delta z=0.05$ m. Examining this figure, it is clear that f_r is a transition frequency. It is the frequency that separates two kinds of behavior for the acoustic waves: propagating waves for $f\geq f_r$ and exponentially decaying sound fields (evanescent waves) for $f<f_r$. The nonstationary signal in the time-wavenumber domain $P(k_x,k_y,z_A,t)$, which is the time evolving pressure in the plane $z=z_A$ at the point k_r of the wavenumber spectrum, will show that its frequency components above the transition frequency propagate as propagating waves and its frequency components below f_r decay exponentially.

IV. DISCRETE FINITE LENGTH IMPULSE RESPONSE

The forward radiation problem is solved by using a convolution in the time-wavenumber domain [see Eq. (25)] between the input acoustic signals and the impulse response in Eq. (26). The accuracy of the instantaneous radiating sources reconstructed from the measurements depends on the sampling rate of the analytical impulse response. It is then very important that the discrete Fourier transform $H_F(\Omega_r,\tau,\omega)$ of the sampled impulse response is close to the theoretical transfer function $H(\Omega_r,\tau,\omega)$. Since the sampled impulse response is not band limited, one more processing stage involving a low-pass filter is added to avoid aliasing effect.

A. Frequency analysis of the sampled impulse response

Here the influence on the sampled impulse response of both parameters Δz the distance between the measurement

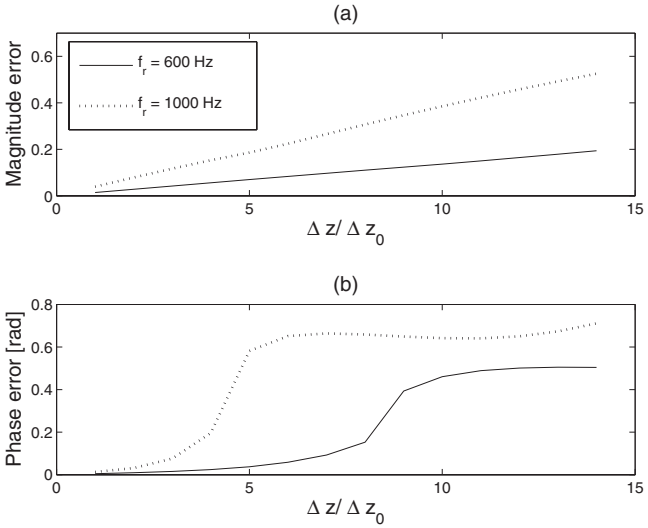

FIG. 4. Errors (a) in the magnitude $E_{|H_F|}$ and (b) in the phase E_{ϕ_F} (rad) of the transfer function $H_F(f)$ as functions of the normalized propagation distance $\Delta z/\Delta z_0$ with $\Delta z_0 = c\Delta t = 0.0215$ m. The transfer function is obtained by applying a Fourier transform to the sampled impulse response in Eq. (26) for $f_e = 16\,000$ Hz and 256 samples.

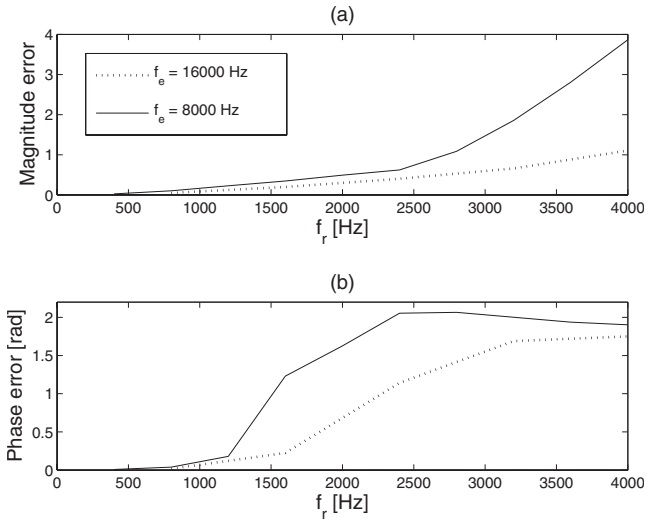

FIG. 5. Errors (a) in the magnitude $E_{|H_F|}$ and (b) in the phase E_{ϕ_F} (rad) of the transfer function $H_F(f)$ as functions of the transition frequency ($\Delta z = 0.043$ m) for two sampling frequencies $f_e = 8000$ Hz ($\Delta z/c\Delta t = 1$) and $f_e = 16\,000$ Hz ($\Delta z/c\Delta t = 2$). 256 samples are considered.

plane and the forward plane, and f_r the transition frequency is investigated. The sampling frequency is f_e and the time interval between successive samples is Δt, the sampling period with $\Delta t = 1/f_e$. The discrete Fourier transform $H_F(\Omega_r, \tau, \omega)$ of the 256 samples of the impulse response $h(\Omega_r, \tau, t)$ is then compared to $H(\Omega_r, \tau, \omega)$. For this purpose, two root mean square errors $E_{|H_F|}$ and E_{ϕ_F} for both the magnitude and the phase of $H_F(\Omega_r, \tau, f) = |H_F(f)|e^{j\phi_F(f)}$ are calculated. They are defined by

$$E_{|H_F|} = \sqrt{\langle (|H(f)| - |H_F(f)|)^2 \rangle}, \tag{31}$$

$$E_{\phi_F} = \sqrt{\langle (\phi(f) - \phi_F(f))^2 \rangle}, \tag{32}$$

where $|H(f)|$ and $\phi(f)$ are the magnitude and the phase of the theoretical transfer function [Eq. (30)] and $\langle\ \rangle$ denotes the average value.

A normalized propagation distance is used here. It is the ratio between the distance Δz and the base distance $\Delta z_0 = c\Delta t = c/f_e$. Both errors in the magnitude and the phase of the transfer function are computed when $\Delta z/\Delta z_0 = \Delta z/c\Delta t$ varies.

1. Influence of the propagation distance on the frequency behavior of the impulse response

The results highlighting the variations in the magnitude and the phase errors as functions of $\Delta z/\Delta z_0$ are given in Fig. 4 for two different transition frequencies: $f_r = 600$ Hz and $f_r = 1000$ Hz. For each normalized distance $\Delta z/\Delta z_0$, the errors are computed according to a transfer function obtained by the discrete Fourier transform of the analytical impulse response sampled at $f_e = 16\,000$ Hz. In this case, $\Delta z_0 = c\Delta t = 0.0215$ m. In Fig. 4(a), for both values of f_r, the error in the magnitude of the transfer function linearly increases as a function of $\Delta z/\Delta z_0$. In Fig. 4(b), for $f_r = 600$ Hz and $f_r = 1000$ Hz, the error in the phase of the transfer function is increasing toward a stable value for $\Delta z/\Delta z_0$ (toward $\Delta z/\Delta z_0 \approx 5$ for $f_r = 1000$ Hz and toward $\Delta z/\Delta z_0 \approx 9$ for $f_r = 600$ Hz) and then remains largely unchanged. The errors in the magnitude and the phase of the transfer function related to the forward radiating problem both increase when the reconstruction plane moves away from the acoustic sources.

It is also noticeable in Fig. 4 that for a given value of $\Delta z/\Delta z_0$, the errors in the magnitude and the phase are higher for $f_r = 1000$ Hz than for $f_r = 600$ Hz. In the next part, the influence of the transition frequency f_r on the frequency behavior of the impulse response is investigated.

2. Influence of the transition frequency on the frequency behavior of the impulse response

The influence of the variations of the transition frequency on the spectral behavior of the impulse response $h(\Omega_r, \tau, t)$ is highlighted in Fig. 5 where the errors in the magnitude and in the phase are represented as functions of f_r for two sampling frequencies applied to $h(\Omega_r, \tau, t)$: $f_e = 8000$ Hz and $f_e = 16\,000$ Hz. Here $\Delta z = 0.043$ m; hence for $f_e = 8000$ Hz, $\Delta z/\Delta z_0 = \Delta z/c\Delta t = 1$ and for $f_e = 16\,000$ Hz, $\Delta z/c\Delta t = 2$. Figure 5 clearly shows that the errors computed in the magnitude and phase both increase as a function of the transition frequency. For $f_e = 16\,000$ Hz, the error in the magnitude in Fig. 5(a) increases almost linearly but remains relatively weak. For $f_e = 8000$ Hz, the error is weak below $f_r = 2400$ Hz but increases very strongly for transition frequencies above. For lower sampling frequencies, the error in the magnitude of the transfer function is more sensitive to the increase in the transition frequency. There is also the same tendency for the error in the phase [see Fig. 5(b)]. The variations in the curves are similar for both sampling frequencies; however, for a given transition frequency, the error is greater for $f_e = 8000$ Hz than for $f_e = 16\,000$ Hz.

For high transition frequencies, the spectral behavior of the impulse response diverges from the theoretical model. Thus, when computing the radiated pressure field, some distorsions may appear due to the convolution between the in-

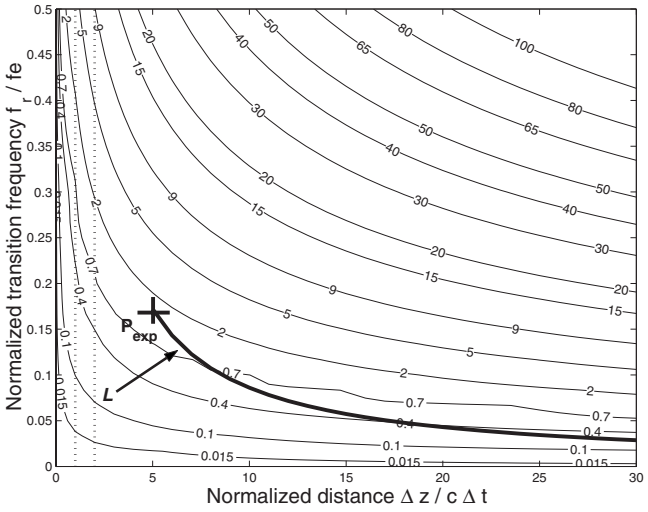

FIG. 6. Error $E_{|H_F|}$ in the magnitude of the transfer function $H_F(f)$ in the plane $(\Delta z/c\Delta t, f_r/f_e)$ and curve (L) giving $f_{r_{\max}}/f_e$ as a function of $\Delta z/c\Delta t$. The configuration parameters are $\Delta z=0.1075$ m, $\Delta L=0.0625$ m, and $f_{r_{\max}}=c/2\Delta L=2752$ Hz. The vertical lines passing by the points $\Delta z/c\Delta t=2$ and $\Delta z/c\Delta t=1$ are shown as dotted lines.

stantaneous wavenumbers resulting from the measurements and the sampled impulse response $h(\Omega_r,\tau,t)$ particularly for large wavenumbers.

3. Influence of the sampling frequency on the frequency behavior of the impulse response

The errors in the magnitude and the phase of the transfer function are now given in a plane $(\Delta z/c\Delta t, f_r/f_e)$ for different sampling frequencies in order to explain the curves in Figs. 4 and 5. Whatever the sampling frequency is chosen, typical maps highlighting isovalue lines are obtained for the error in the magnitude (see Fig. 6) and for the error in the phase (see Fig. 7). It is noticeable that the choice of two normalized values f_r/f_e and $\Delta z/\Delta z_0=\Delta z/c\Delta t$ leads to the same errors in both magnitude and phase of the transfer function computed by the Fourier transform of the sampled impulse response whatever the sampling rate f_e used. 256 samples are considered for the impulse response.

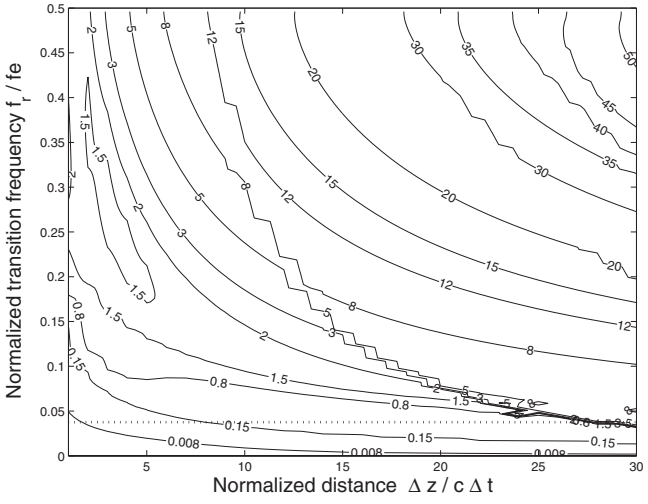

FIG. 7. Error E_{ϕ_F} (rad) in the phase of the transfer function $H_F(f)$ in the plane $(\Delta z/c\Delta t, f_r/f_e)$. The horizontal line passing by the point $f_r/f_e=0.0375$ is shown as a dotted line.

The tendency of the phase error curve in Fig. 4(b) obtained for $f_r=600$ Hz can be explained by drawing in Fig. 7 a virtual horizontal straight line passing by the point $f_r/f_e=600/16\,000=0.0375$. When $\Delta z/\Delta z_0$ varies from 0 to 15, the line first crosses several isovalues of the error, which justifies the increasing part of the curve in Fig. 4(b), and then the line becomes tangent to an isovalue, which explains the constant behavior from $\Delta z/\Delta z_0\approx 9$ in Fig. 4(b). The plot of the error in the magnitude in Fig. 6 helps to explain the variations in Fig. 5(a). Indeed by drawing a virtual vertical straight line passing by the point $\Delta z/c\Delta t=2$ in Fig. 6, one can read the values taken by the curve in Fig. 5 for $f_e=16\,000$ Hz. These values are provided by the intersection between the vertical straight line and the isovalues of the error from $f_r/f_e=0$ to $f_r/f_e=4000/16\,000=0.25$. The curve in Fig. 5 for $f_e=8000$ Hz is given by the intersection in Fig. 6 between the vertical straight line passing through point $\Delta z/c\Delta t=1$ (drawn from $f_r/f_e=0$ to $f_r/f_e=4000/8000=0.5$) and the isovalue errors.

The aim of the study is now to investigate the influence of an increase in the sampling frequency for a given numerical setup. For the acquisition stage, the step size in both x and y directions is $\Delta L=0.0625$ m. The sampling frequency is $f_e=16\,000$ Hz and the propagation distance is set to $\Delta z=0.1075$ m. The maximum transition frequency allowed which fulfills the Shannon condition of space sampling is

$$f_{r_{\max}}=\frac{ck_{\max}}{2\pi}, \tag{33}$$

with $k_{\max}=\pi/\Delta L$, the wavenumber limit.

Finally $f_{r_{\max}}$ can be written as

$$f_{r_{\max}}=\frac{c}{2\Delta L}. \tag{34}$$

It is also true that the maximum transition frequency must fulfill the Shannon condition in the time domain. In fact, the smallest value of the couple of values $(f_e/2, c/2\Delta L)$ must be chosen for $f_{r_{\max}}$. For this numerical setup, $f_{r_{\max}}=\min(8000\text{ Hz}, 2752\text{ Hz})=2752$ Hz.

In this configuration, the transition frequency varies from 0 to $f_{r_{\max}}=c/2\Delta L=2752$ Hz. Thus, if f_e is not lower, the error values in the area $f_r/f_e>f_{r_{\max}}/f_e$ in Figs. 6 and 7 will never be reached. It is also interesting to observe the values of the error when the sampling frequency increases.

$f_{r_{\max}}/f_e$ can be written as

$$\frac{f_{r_{\max}}}{f_e}=\frac{C_{\exp}}{\Delta z/c\Delta t}, \tag{35}$$

where $C_{\exp}=f_{r_{\max}}\Delta z/c$ is a constant term depending on the numerical or experimental setup. Here $C_{\exp}=\Delta z/2\Delta L=0.86$. Thus, the values taken by $f_{r_{\max}}/f_e$ are given by $0.86/(\Delta z/c\Delta t)$. The numerical setup ($f_e=1/\Delta t=16\,000$ Hz, $\Delta z=0.1075$ m, $\Delta L=0.0625$ m) provides the coordinates of $P_{\exp}$ (see Fig. 6) the first point of the curve L defined by $f_{r_{\max}}/f_e=0.86/(\Delta z/c\Delta t)$ in the plane $(\Delta z/c\Delta t, f_r/f_e)$: $P_{\exp}(\Delta z/c\Delta t, f_{r_{\max}}/f_e)=P_{\exp}(5, 0.172)$. When f_e is increased

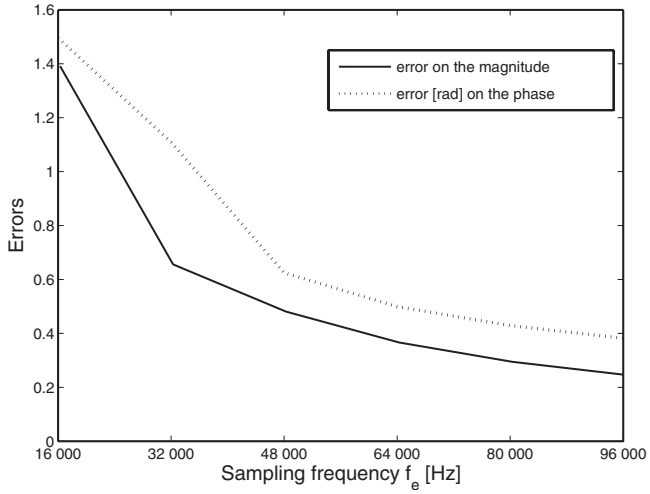

FIG. 8. Errors in the magnitude and in the phase (rad) of the transfer function $H_F(f)$ as functions of the sampling frequency f_e for the transition frequency f_r=2752 Hz and the propagation distance Δz=0.1075 m.

from 16 000 to 96 000 Hz, the curve L decreases and crosses the isovalue lines toward the decreasing error values. It can be concluded that an increase in the sampling frequency causes the errors to decrease for each impulse response $h(\Omega_r,\tau,t)$ of the filters used in the time-wavenumber domain to solve the radiation problem. The sampling frequency can be increased at the acquisition stage or *a posteriori* with a Shannon interpolation of the sampled signal.

The reduction in the errors when the sampling frequency increases is shown in Fig. 8, where the errors in both magnitude and phase are obtained from the previous numerical setup: Δz=0.1075 m and f_r=2752 Hz. These values are collected from the isovalue lines crossed by the curve L in Fig. 6.

The fact that an increase in the sampling frequency leads to a reduction in the errors in both magnitude and phase of the transfer function has been highlighted. However, even if the use of a high sampling frequency seems necessary, it is not sufficient, which is illustrated in Fig. 9. In this figure, the

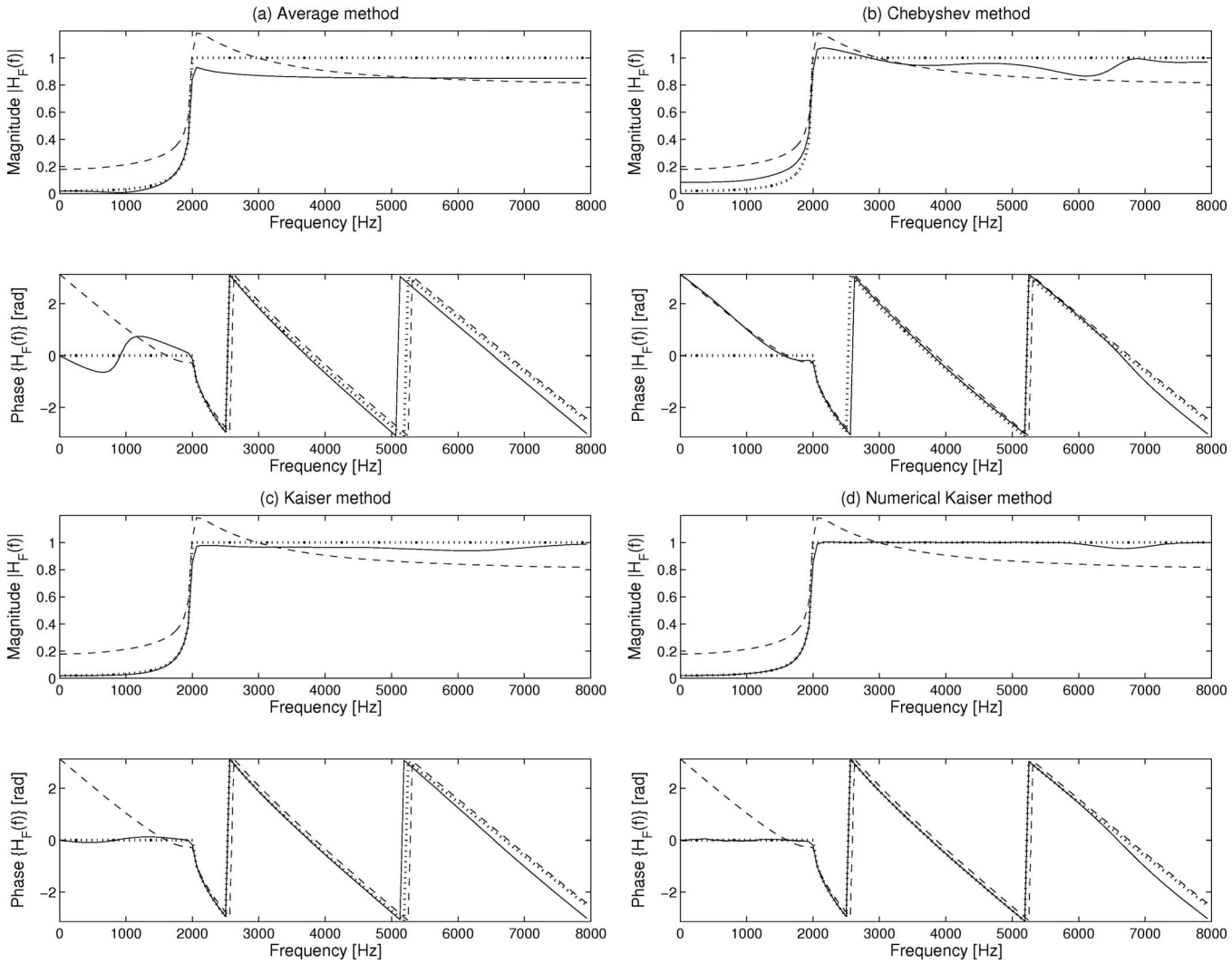

FIG. 9. Transfer functions $H_F(\Omega_r,\tau,f)$ shown as solid lines (magnitude and phase in rad) after processing $h(\Omega_r,\tau,t)$. N=256 points, f_e=16 000 Hz, Δz =0.1075 m ($\Delta z/c\Delta t$=5), and f_r=2000 Hz (f_r/f_e=0.125). The theoretical transfer function $H(\Omega_r,\tau,f)$ is indicated as a dotted line. The Fourier transform of $h(\Omega_r,\tau,t)$ sampled at f_e=64 000 Hz is shown as a dashed line. (a) Sampling h using the average method, (b) Chebyshev method (cutoff frequency f_c =6400 Hz and upsampling factor of D=8), (c) low-pass filtering using a Kaiser–Bessel filter (f_c=6640 Hz and D=2), and (d) numerical Kaiser method (f_c=6780 Hz).

transfer function (magnitude and phase) $H_F(\Omega_r,\tau,f)$ computed by Fourier transform of $h(\Omega_r,\tau,t)$ is drawn as a dashed line for $f_e=64\,000$ Hz, $\Delta z=0.1075$ m [i.e., $(\Delta z/c\Delta t)=20$] and $f_r=2000$ Hz [i.e., $f_r/f_e=0.031\,25$]. For these two values $(\Delta z/c\Delta t, f_r/f_e)$, the error in the magnitude is $E_{|H_F|}=0.2$ and the error in the phase is $E_{\phi_F}=0.45$ (the values can also be extracted from Figs. 6 and 7). The use of a high sampling frequency applied to the impulse response is advantageous because $E_{|H_F|}=0.6$ and $E_{\phi_F}=1.3$ for $f_e=16\,000$ Hz. However, the result is not satisfactory, as shown in Fig. 9, where the transfer function, shown as a dashed line, is far from the theoretical model, shown as a dotted line. This result leads us to consider additional processing of the impulse response in order to provide the pressure field radiated by the acoustic sources on a forward plane. These processing techniques are detailed in Sec. IV B.

B. Processing for providing an operational impulse response

Two approaches are considered here. The first is based on the analytical formulation of the impulse response $h(\Omega_r,\tau,t)$ given in Eq. (26) in the time-wavenumber domain. The second starts from the theoretical frequency response $H(\Omega_r,\tau,\omega)$ in Eq. (30) and by using an inverse Fourier transform yields the impulse response.

1. Processing from the analytical impulse response

For this case, consider the following equation derived from Eq. (26) giving the impulse response:

$$h(\Omega_r,\tau,t)=\delta(t-\tau)-g(\Omega_r,\tau,t), \tag{36}$$

where

$$g(\Omega_r,\tau,t)=\pi\Omega_r^2\frac{J_1(\Omega_r\sqrt{t^2-\tau^2})}{\Omega_r\sqrt{t^2-\tau^2}}\Gamma(t-\tau). \tag{37}$$

As sampling the impulse response even with a relatively high rate may lead to distorsions in the transfer function, direct sampling is replaced by average sampling. Instead of considering $g[n]$, the sampling value of $g(t)$ at the time $t=n\Delta t$, the average value $\bar{g}[n]$ is computed into an interval Δt centered at $t=n\Delta t$:

$$\bar{g}[n]=\frac{1}{\Delta t}\int_{n\Delta t-(\Delta t/2)}^{n\Delta t+(\Delta t/2)}g(t)dt. \tag{38}$$

The integral in Eq. (38) is approximated by the trapezoidal formula.

Another modification is used to overcome the problem of the impulse response whose transfer function is not band limited. The process consists first of increasing the sampling rate of the impulse response by a factor D so that the new sampling frequency is $f_e'=Df_e$. The response contains DN samples. Then the upsampled response is filtered using a low-pass filter. Finally, the filtered impulse response is downsampling by the factor $1/D$ to ensure that the final sampling frequency f_e'/D matches f_e, that of the acoustic signals acquired. The number of samples of the resulting impulse response is N.

The use of two low-pass filters have been investigated, one with an infinite impulse response, a Chebyshev filter, and the other one with a finite impulse response (FIR) given by associating a cardinal sine with a Kaiser–Bessel window.[16] The choice of a Chebyshev filter which exhibits equiripple behavior in the passband and a monotonic characteristic in the stopband facilitates the implementation. The advantage of the FIR filter is that it has a linear-phase characteristic within the passband. Then it is easy to postprocess the filtered impulse response to recover the phase. In addition, the Kaiser–Bessel window which decays toward zero gradually permits to alleviate the presence of large oscillations in both the passband and the stopband of the frequency response.

The impulse response of the FIR filter is

$$w(t)=\frac{I_0(\beta\sqrt{1-(2t/T)^2})}{I_0(\beta)}\frac{\sin(\alpha\pi tf_e)}{\pi t}. \tag{39}$$

I_0 is the modified Bessel function of the first kind and order 0. T is the duration of the Kaiser–Bessel window. α is linked to the cutoff frequency f_c of the low-pass filter and β is a shape parameter of the Kaiser–Bessel window:

$$\alpha=\frac{2f_c}{f_e}, \tag{40}$$

$$\beta\approx 0.1102(A-8.7), \tag{41}$$

where A is the sidelobe attenuation in decibels.

Two ways of implementing the convolution between the impulse response and the low-pass filter can be considered. First, the filtered response $g_f(t)$ can be provided using a discrete sum as

$$g_f[n]=\sum_m w[m]g[n-m]. \tag{42}$$

But it can be also computed using a numerical approximation of the following integral given by the trapezoidal method:

$$g_f(t)=\int_{t-T/2}^{t+T/2}g(\theta)w(t-\theta)d\theta. \tag{43}$$

2. Processing from the theoretical frequency response

The Fourier transform of Eq. (36) yields

$$H(\Omega_r,\tau,\omega)=e^{-j\omega\tau}-G(\Omega_r,\tau,\omega). \tag{44}$$

Since $H(\Omega_r,\tau,\omega)$ is analytically defined in Eq. (30), so it is for the transfer function $G(\Omega_r,\tau,\omega)$ whose both theoretical magnitude and phase are easily deduced.

It follows

$$G(\Omega_r,\tau,\omega)=e^{-j\omega\tau}-H(\Omega_r,\tau,\omega). \tag{45}$$

By applying an inverse Fourier transform either to $H(\Omega_r,\tau,\omega)$ [Eq. (30)] or to $G(\Omega_r,\tau,\omega)$ [Eq. (45)], the im-

pulse response $h(\Omega_r,\tau,t)$ or $g(\Omega_r,\tau,t)$ is obtained. From Eq. (36), both approaches provide finally the same impulse response $h(\Omega_r,\tau,t)$.

C. Comparisons between transfer functions resulting from processing

The aim of this part is to compare several transfer functions $G(\Omega_r,\tau,\omega)$ resulting from different processing techniques in order to evaluate their effectiveness in resolving the source radiating problem. Four treatments are applied to the theoretical function $g(\Omega_r,\tau,t)$ in Eq. (37). They are summarized as follows.

- *Average method.* $g(\Omega_r,\tau,t)$ is average sampled according to Eq. (38).
- *Chebyshev method.* $g(\Omega_r,\tau,t)$ is low-pass filtered using a Chebyshev filter with a cutoff frequency $f_c=6400$ Hz. It is achieved by upsampling $g(\Omega_r,\tau,t)$ by the factor $D=8$ using the low-pass filter and then downsampling the resulting response by the factor $1/D$.
- *Kaiser method.* $g(\Omega_r,\tau,t)$ is average sampled and low-pass filtered using a Kaiser–Bessel filter with a cutoff frequency $f_c=6640$ Hz. An upsampling factor of $D=2$ is used.
- *Numerical Kaiser method.* The same Kaiser–Bessel filter is applied but the integral in Eq. (43) is numerically computed using the trapezoidal method.

For all cases, $g(\Omega_r,\tau,t)$ is initially sampled with the sampling frequency $f_e=16\,000$ Hz giving 256 samples. The propagation distance and the transition frequency are set to $\Delta z=0.1075$ m and $f_r=2000$ Hz. Figure 9 highlights the transfer functions $H(\Omega_r,\tau,f)$ (magnitude and phase) for the four different processing techniques. The frequency responses are obtained by applying a Fourier transform to the sampled response $g(\Omega_r,\tau,t)$ before using Eq. (44).

By comparing the four transfer functions to the dashed line (see Fig. 9), it seems evident that the transfer functions provided by processing $g(\Omega_r,\tau,t)$ are more relevant than the one obtained by operating a Fourier transform directly on the sampled response even though the sampling frequency is higher (64 000 Hz instead of 16 000 Hz). In addition, filtering $g(\Omega_r,\tau,t)$ in order to limit its frequency band is advantageous. The use of average sampling with no filter is less effective than filtering, in particular, in the frequency area of propagating components. The use of a FIR filter with a Kaiser–Bessel window seems more accurate than the use of a Chebyshev filter especially for the phase. The most accurate transfer function in Fig. 9 is obtained by numerically computing the integral of convolution involving the Kaiser–Bessel filter. One can note that this comparison must be done for each transition frequency and then for each point of the wavenumber domain.

These remarks can also be verified by considering the variations in the magnitude and phase errors of Eqs. (31) and (32) when the transfer functions $H_F(f)$ are computed from the Chebyshev, the average, the Kaiser, and the numerical Kaiser methods. For this purpose, Figs. 10 and 11 are to be compared with Figs. 4 and 5. It is clear that processing the impulse response leads to a reduction in the errors. The lowest errors are achieved by using the numerical Kaiser method while the Chebyshev method seems to generate phase errors (see Fig. 10) when the propagation distance increases. Increasing the sampling rate of the impulse response by a factor higher than 8 could enhance the performance of the Chebyshev method.

It is of course true that the best matching between the theoretical and the computed transfer functions occurs for the method based on the inverse Fourier transform (see Sec. IV B 2), which is evident as the starting point of the approach, called here Fourier method, is precisely the theoretical frequency response.

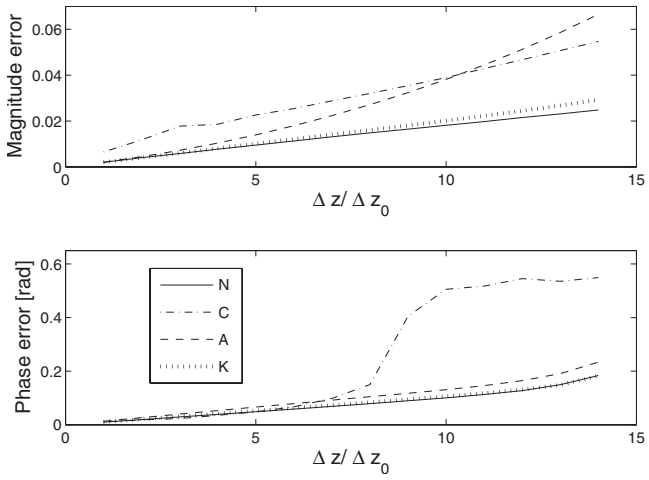

FIG. 10. Errors in the magnitude $E_{|H_F|}$ and in the phase E_{ϕ_F} (rad) of the transfer function $H_F(f)$ as functions of the normalized propagation distance $\Delta z/\Delta z_0$ with $\Delta z_0=c\Delta t=0.0215$ m. The normalized transition frequency is $f_r=1000$ Hz. The transfer functions are obtained by applying the Fourier transform to the impulse responses computed by Chebyshev (C), average (A), Kaiser (K) and numerical Kaiser (N) methods for $f_e=16\,000$ Hz.

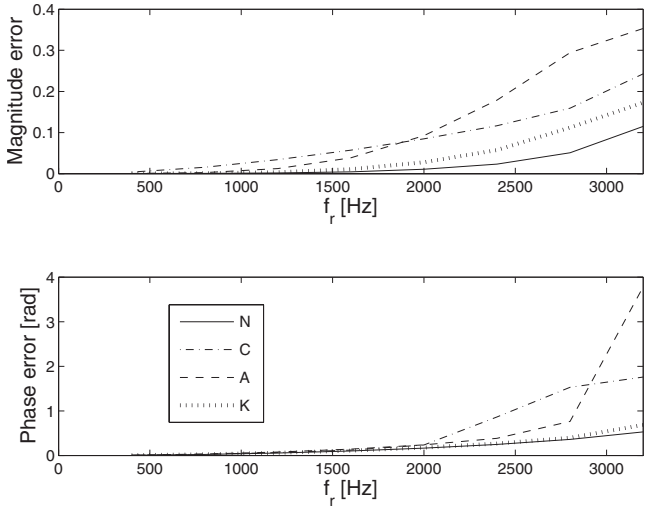

FIG. 11. Errors in the magnitude $E_{|H_F|}$ and in the phase E_{ϕ_F} (rad) of the transfer functions $H_F(f)$ as functions of the transition frequency ($\Delta z=0.043$ m) for $f_e=8000$ Hz ($\Delta z/c\Delta t=1$). The transfer functions are obtained by applying the Fourier transform to the impulse responses computed by Chebyshev (C), average (A), Kaiser (K), and numerical Kaiser (N) methods.

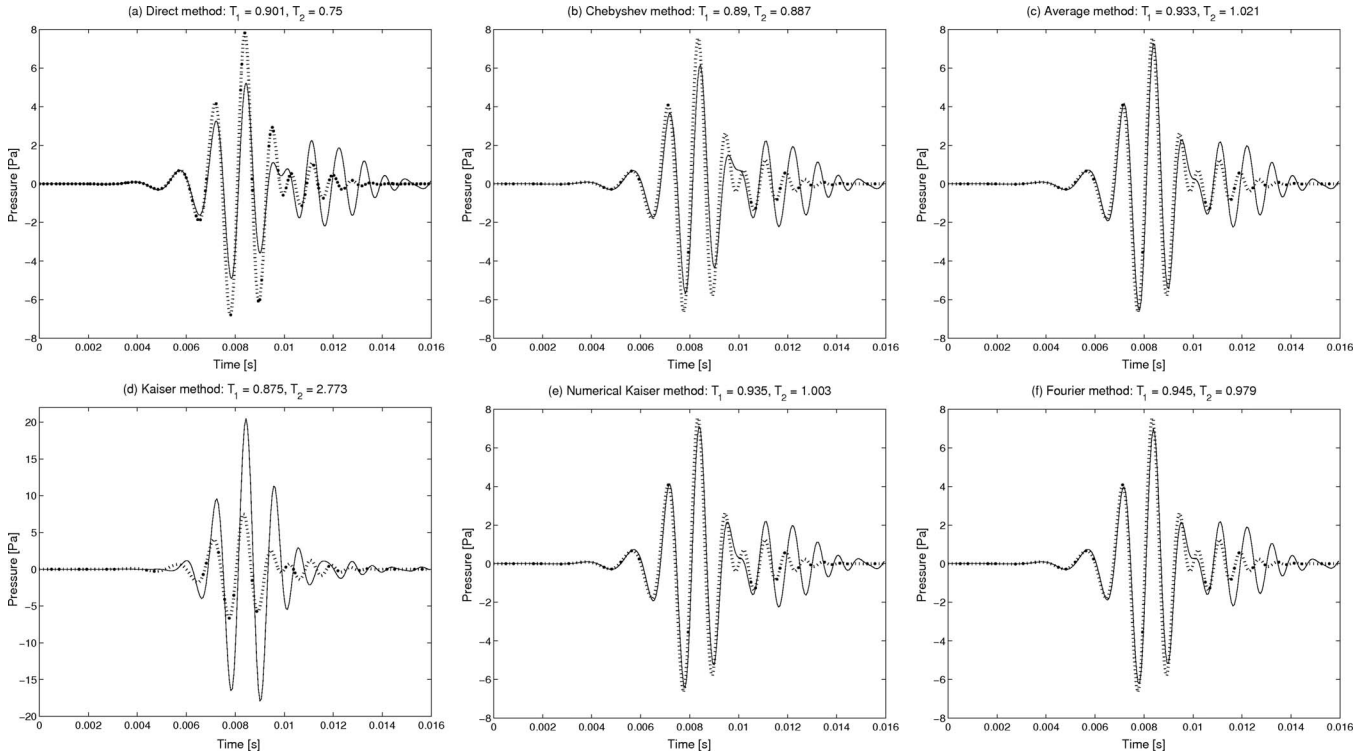

FIG. 12. Reconstructed temporal signals (solid line) versus reference signals (dotted line) in the time-space domain in location P_3 (see Fig. 1) for different impulse responses computed by six methods [direct (a), Chebyshev (b), average (c), Kaiser (d), numerical Kaiser (e), and Fourier (f)]. The indicators T_1 [Eq. (47)] and T_2 [Eq. (48)] are given on top of each graph.

V. NUMERICAL RESULTS

A. Setup

The source plane is composed of three monopoles at the positions M_1 (0.3125 m, 0.375 m, 0 m), M_2 (0.75 m, 0.75 m, 0 m), and M_3 (0.25 m, 0.75 m, 0 m). Both monopoles M_1 and M_2 generate a signal with a linear frequency modulation in the band [200 Hz, 1800 Hz] and a Gaussian amplitude modulation while monopole M_3 radiates a Morlet wavelet whose expression is

$$s(t) = \cos(2\pi f_0 t)e^{-t^2/2}, \tag{46}$$

with $f_0=800$ Hz. Thus the sources are nonstationary. The simulation of the acquisition is done using a 17×17 microphone array located in the measurement plane $z=z_A$ with $z_A=0.05$ m. The step size in both x and y directions is $\Delta L=0.0625$ m, providing an overall aperture size of 1.0×1.0 m^2. The propagation distance is $\Delta z=0.1075$ m. Thus, the forward plane is located at $z_F=0.1575$ m, as shown in Fig. 1. The emitted signals are sampled at a frequency of $f_e=16\,000$ Hz providing 256 samples.

The aim of this study is to reconstruct the time evolving pressure field at each point of the forward plane in front of the square grid of 17×17 virtual microphones using Eq. (25). Five different impulse responses $h(\Omega_r,\tau,t)$ in the time-wavenumber domain are investigated. They are computed from the Chebyshev method, the Kaiser method, the numerical Kaiser method, the Fourier method, and the direct method for which the impulse response $h(\Omega_r,\tau,t)$ is provided by directly sampling $g(\Omega_r,\tau,t)$ in Eq. (37) at $f_e=64\,000$ Hz.

B. Indicators

In order to comment the results obtained objectively, two temporal indicators T_1 and T_2 are proposed [see Eqs. (47) and (48)]. They are based on the reconstructed signals $p(x,y,z_F,t)$ but also on simulated signals $p_r(x,y,z_F,t)$ directly propagated on the forward plane $z=z_F$, which are considered as reference signals:

$$T_1 = \frac{\langle p_r(x,y,z_F,t)p(x,y,z_F,t)\rangle}{\sqrt{\langle p_r^2(x,y,z_F,t)\rangle\langle p^2(x,y,z_F,t)\rangle}}, \tag{47}$$

$$T_2 = \sqrt{\frac{\langle p^2(x,y,z_F,t)\rangle}{\langle p_r^2(x,y,z_F,t)\rangle}}. \tag{48}$$

$\langle\ \rangle$ is the average value.

T_1 is a correlation coefficient which is sensitive to the similarity between the shapes of the signals and thus between their phase difference. T_2 is the ratio between two root mean square values for characterizing the similarity of the amplitudes of both signals.

C. Results in the time-space domain

Figure 12 highlights the temporal pressure signals $p(0.25\text{ m},0.75\text{ m},0.1575\text{ m},t)$ radiated in P_3 whose location is indicated in Fig. 1. P_3 is in front of the monopoles M_3. The pressure signals are provided by the method proposed using the five different impulse responses in the time-wavenumber domain mentioned above plus the impulse response obtained by the inverse Fourier transform. They are compared to the reference pressure signals directly propagated to the forward

plane $z=z_F$ by simulation. The indicator values T_1 and T_2 are reported in Table I. The examination of both Fig. 12 and Table I leads to the ranking of the methods in order of increasing relevance: Kaiser method (K), direct method (D), average method (A), Chebyshev method (C), numerical Kaiser method (N), and Fourier method (F). The Kaiser method seems to suffer from a two weak oversampling factor of 2. Therefore, the use of a low-pass Kaiser–Bessel filter with a numerical implementation or the inverse Fourier transform of the analytical transfer function leads to the most operational impulse response in the time-wavenumber domain. In addition, the Fourier method is more efficient than the numerical Kaiser method.

Results are enhanced when the impulse response $h(\Omega_r,\tau,t)$ is low-pass filtered. It confirms the fact that $g(\Omega_r,\tau,t)$ in Eq. (37) should not only be sampled. With filtering or using the Fourier transform, results are improved in the whole space, which can be verified by comparing the

TABLE I. Indicators T_1 [Eq. (47)] and T_2 [Eq. (48)] computed from reference signals and pressure signals computed in $z=z_F$ from impulse responses obtained by the direct method (D), the Kaiser method (K), the average method (A), the Chebyshev method (C), the numerical Kaiser method (N), and the Fourier method (F).

			P_2			
	D	K	A	C	N	F
T_1	0.929	0.944	0.958	0.920	0.961	0.963
T_2	0.812	2.397	1.054	0.951	1.009	0.971
			P_3			
	D	K	A	C	N	F
T_1	0.901	0.875	0.933	0.890	0.935	0.945
T_2	0.750	2.773	1.021	0.887	1.003	0.979
			P_4			
	D	K	A	C	N	F
T_1	0.991	0.689	0.989	0.990	0.989	0.991
T_2	1.022	1.025	1.056	1.043	1.063	1.063

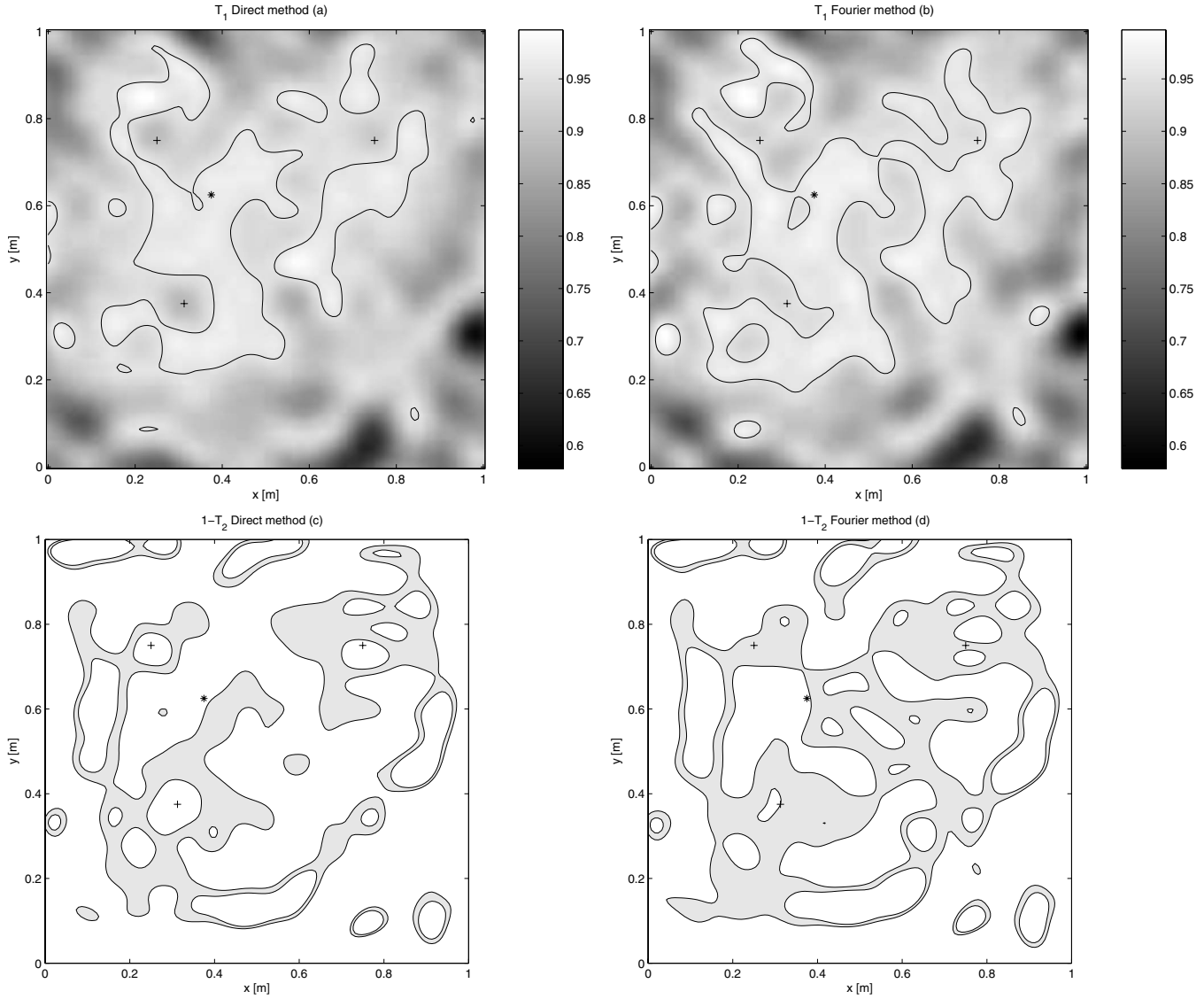

FIG. 13. Spatial maps of indicator T_1 and $1-T_2$ to assess the phase and the amplitude similarities between the reference signals and the projected signals using the direct method [(a) and (c)] with the sampling frequency $f_e=64\,000$ Hz and the Fourier method [(b) and (d)] with $f_e=16\,000$ Hz. The locations of $P_1(+)$, $P_2(+)$, $P_3(+)$, and $P_4(*)$ are marked. [(a) and (c)] The contour line is at the value 0.95. [(c) and (d)] The areas in gray correspond to values of $1-T_2$ within the interval $[-0.05,0.05]$.

reconstructed temporal signals from other locations of the space with the reference signals as in Fig. 12. For this purpose, spatial cartographies are reported for the direct method and the Fourier method in Fig. 13. The 0.95 contour line is displayed for indicator T_1 in Figs. 13(a) and 13(b). One can observe that the locations facing the monopoles do not give the best results in terms of phase difference. However, the error obtained by directly sampling the impulse response with $f_e=64\,000$ Hz is decreased when the Fourier method is applied even with a lower sampling frequency ($f_e=16\,000$ Hz). The error is also higher near the edges of the scanned area. In Figs. 13(c) and 13(d), the spatial map is given for indicator $1-T_2$. Indeed the similarity between the amplitudes of the reference signals and the projected signals is evident when $1-T_2$ is close to 0. In fact, the lowest error is reached for spatial locations within the area in gray for $1-T_2$ values in the interval $[-0.05,0.05]$. It is noticeable that this area is larger for the Fourier method than from the direct method. In most locations, the amplitudes of the projected signals are overestimated. However, the amplitudes of the projected signals are inclined to be underestimated by the direct method for locations around the source monopoles. The Fourier method gives better results near the monopoles. In the same way as the spatial map for indicator T_1, the error for $1-T_2$ is higher near the border of the antenna.

VI. CONCLUSION

The method proposed to forward propagate time-evolving acoustic fields has the singularity to be based on a convolution product in the time-wavenumber domain involving an analytical impulse response. However, this impulse response needs to be carefully implemented. Indeed, it is shown here that just sampling the response is not sufficient to deduce the time-dependent pressure field radiated by the sources. Two processing methods give accurate results. The first method applies a Kaiser–Bessel low-pass filter to the impulse response which is average sampled and the convolution integral is numerically computed using the trapezoidal technique. The second method provides the impulse response by computing an inverse Fourier transform of the analytical transfer function.

The errors made on the propagated acoustic fields increase with the distance separating the sources from the reconstructed plane and also with the increase in a specific parameter, the transition frequency which depends on each wavenumber and separates two tendencies of the travelling waves: propagating waves and evanescent waves. It is clear that upsampling the impulse response reduces the errors. It is remarkable that whatever the sampling frequency, the propagation distance, or the transition frequency chosen, the errors are the same as long as the normalized frequency (of the transition frequency by the sampling frequency) and the normalized distance (of the propagation distance by the distance covered during a sampling step) remain constant.

The main interest of the method is that it provides the instantaneous acoustic field radiated from the sources. The approach could be applied to active control and to diagnose and monitor various acoustic systems and to calculate the radiation from structures under unsteady excitations such as those produced by impacts or turbulent flows.

[1] S. G. Hill, S. D. Snyder, and B. S. Cazzolato, "Deriving time-domain models of structural-acoustic radiation into free space," Mech. Syst. Signal Process. **19**, 1015–1033 (2005).

[2] S. J. Elliott and M. E. Johnson, "Radiation modes and the active control of sound power," J. Acoust. Soc. Am. **94**, 2194–2204 (1993).

[3] A. Chaigne and C. Lambourg, "Time-domain simulation of damped impacted plates. i. theory and experiments," J. Acoust. Soc. Am. **109**, 1422–1432 (2001).

[4] G. Derveaux, A. Chaigne, P. Joly, and E. Bécache, "Time-domain simulation of a guitar: model and method," J. Acoust. Soc. Am. **114**, 3368–3383 (2003).

[5] A. Akay and M. Latcha, "Sound radiation from an impact-excited clamped circular plate in an infinite baffle," J. Acoust. Soc. Am. **74**, 640–648 (1983).

[6] P. Troccaz, R. Woodcock, and F. Laville, "Acoustic radiation due to the inelastic impact of a sphere on a rectangular plate," J. Acoust. Soc. Am. **108**, 2197–2202 (2000).

[7] E. G. Williams, *Fourier Acoustics: Sound Radiation and Nearfield Acoustical Holography* (Academic, New York, 1999).

[8] J.-H. Thomas, V. Grulier, S. Paillasseur, J.-C. Pascal, and J.-C. Le Roux, "Real-time nearfield acoustic holography (RT-NAH): A technique for time-continuous reconstruction of a source signal," in Proceedings of Novem 2005, Saint-Raphaël, France (2005), Paper No. 139.

[9] M. C. Junger and D. Feit, *Sound, Structures, and Their Interaction* (MIT, Cambridge, MA, 1986) (republication by the Acoustical Society of America, 1993).

[10] E. G. Williams and J. D. Maynard, "Numerical evaluation of the rayleigh integral for planar radiators using the FFT," J. Acoust. Soc. Am. **72**, 2020–2030 (1982).

[11] O. de la Rochefoucauld, M. Melon, and A. Garcia, "Time domain holography: Forward projection of simulated and measured sound pressure fields," J. Acoust. Soc. Am. **116**, 142–153 (2004).

[12] M. Forbes, S. Letcher, and P. Stepanishen, "A wave vector, time-domain method of forward projecting time-dependent pressure fields," J. Acoust. Soc. Am. **90**, 2782–2792 (1991).

[13] V. Grulier, "Propagation directe et inverse dans l'espace temps-nombre d'onde: Application à une méthode d'holographie acoustique de champ proche pour les sources non stationnaires (Direct and inverse propagation in the time-wavenumber domain: Application to a nearfield acoustic holography method for non stationary sources)," Thesis of the Université du Maine, Le Mans, France (2005).

[14] V. Grulier, J.-H. Thomas, J.-C. Pascal, and J.-C. Le Roux, "Time varying forward projection using wavenumber formulation," Proceedings of Internoise2004, Prague, Czech Republic (2004), Paper No. 406.

[15] J. Hladik, *La transformation de Laplace à plusieurs variables (The Multi-Variable Laplace Transform)* (Masson, Paris, 1969).

[16] A. V. Oppenheim, R. W. Schafer, and J. R. Buck, *Discrete-Time Signal Processing*, 2nd ed. (Prentice-Hall, Upper Saddle River, NJ, 1999).